IMA Journal of Applied Mathematics (1999) **63**, 217–246

Vacuum moulding of a superplastic in two dimensions

S. J. CHAPMAN
Mathematical Institute, 24–29 St. Giles, Oxford OX1 3LB
A. D. FITT
Faculty of Mathematical Studies, University of Southampton, Southampton SO17 1BJ
AND
G. C. PULOS
Instituto de Investigaciónes en Materiales, UNAM, Apdo. Postal 70-360*, Circuito Exterior, Cd. Universitaria* 04510 *– México, D.F., México*

[Received 13 March 1998]

A mathematical model is proposed for the process of vacuum superplastic forming. The model exploits the fact that in most industrial applications the sheet aspect ratio (thickness/sheet width) is small. After an initial consideration of some of the more general properties and the literature of superplastic materials, the elastic/plastic deformation of an internally-inflated thin-walled cylinder is examined. Plates of arbitrary geometry are then considered. A quasisteady model in which the sheet moves through a sequence of steady states is developed. Some simplified closed-form solutions are examined, but for general cases a system of nonlinear partial differential equations must be solved numerically. An efficient and accurate semi-explicit numerical scheme is proposed and a simplified stability analysis is presented; the method is then used to compute properties of superplastic vacuum moulded sheets in a number of practically motivated cases.

1. Introduction

Superplasticity in metals and alloys is a phenomenon that has attracted the attention of members of the scientific and industrial communities for at least 30 years. More recently, superplastic behaviour has been studied in intermetallics (whose crystal structures and properties often differ markedly from those of their constituents), ceramics and metal matrix composites.

Superplastic behaviour is characterized by the presence of very large (plastic) deformations. Strains of order 2 are typical but in many materials the strain may reach 10 or 20. (The industry traditionally refers to such deformations as being 200 to over a few thousand 'per cent'.) This is in marked contrast to normal plastic deformations which typically range from less than 1 per cent to about 80 per cent. From a materials science point of view the requirement for superplasticity in a given material is that its grain size is small (typically less than 10 microns). When this is so, for temperatures of approximately half of the melting temperature (in degrees C) and for deformation rates of between 10^{-3}/s for grain sizes of 10 microns and 10/s for 0·5 micron grains (Sherby *et al.* (1994)), materials are able to undergo large deformations without failure. The micromechanical details of exactly how

superplastic deformations occur are complex. By general consensus, however, the most important mechanism at work is that the small grain size allows grain boundary sliding to occur while cavitation is delayed. Void formation and coalescence as a precursor to microcracking (a typical failure mechanism in ductile materials) is thus avoided.

From an industrial point of view, superplasticity brings several advantages to material forming technology. The manufacture of complex shaped pieces may be accomplished with low pressures, without any welding and with minimal or no subsequent machining. As with any thin-walled structure, the strength and failure load (under buckling, for example) depend critically on the local curvature and thickness.

The motivation for the model developed in this study arises from the developmental work of Professor Torres (Instituto de Investigaciónes en Materiales, UNAM, Mexico City) which has been carried out on two superplastic alloys. The materials used in the experiments were a cadmium–zinc alloy and zinalco, a 77 per cent zinc, 21 per cent aluminum and 2 per cent copper alloy developed by Professor Torres and his group. Experiments were carried out on the behaviour of hemispheric free-bulging from sheets as well as vacuum moulding in a circular cylindrical mould with a depth between 1 and 1·3 cylinder diameters (giving deformations of approximately 200 to 250 per cent). The hemispherical bulging may be considered as the first part of a commercial vacuum moulding experiment where the superplastic has not reached the walls of the mould.

The objective of the current study is to develop a model for simulating the superplastic forming process which will also predict the thickness distribution. Other questions of interest are the deflection of the sheet as a function of pressure for a given mould opening, and the deflection as a function of mould diameter for a given pressure.

We begin by describing the configuration under consideration and the modelling assumptions that will be made. Consider a flat sheet of metal of initial uniform thickness d clamped to the edges of a two-dimensional mould (that is, a channel) of width $2a$ and depth b (typically $d \sim 0{\cdot}02a$). We assume that the pressure inside the mould is maintained at P_2, whilst outside the mould $P = P_1 > P_2$. Figure 1 shows a schematic diagram of the arrangement. For small pressure differences this configuration has been much studied. It amounts essentially to a flat plate in which the out of plane loading (uniform pressure) is resisted by bending stresses (in-plane stresses); the concave surface of the plate is under compression whilst the convex surface is under tension. This initial configuration problem may be described by standard linear plate theory, valid when the deflections are less than the thickness of the plate.

Assume now that the pressure in the mould is further decreased. For the greater deflections that now result a more refined theory is required. Nonlinear plate theories for such circumstances are well established (see, for example Green & Zerna (1954)); in the current case, the out-of-plane loads are carried by in-plane bending stresses in combination with membrane (that is, tensile) hoop stresses.

Now suppose that the mould pressure is decreased still further. As the deformation of the material increases, even nonlinear plate theory eventually becomes invalid. Experimentally, a plastic ‘hinge’ forms on the rim of the mould. Shell theory, in which a curved geometry can carry out-of-plane loads by hoop stresses (positive throughout the thickness) is now applicable.

The effect of plastic hinge formation may be understood by considering a cantilever

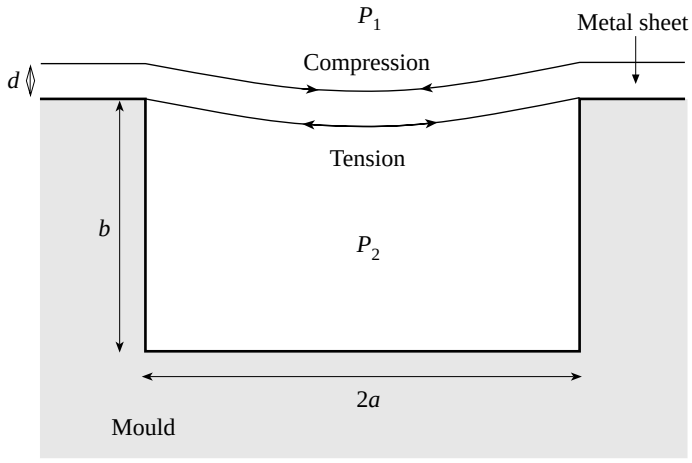

FIG. 1. The geometry of the sheet ($P_1 > P_2$)

beam under a uniform pressure. At a certain critical pressure plastic zones are formed at the built-in end. Such zones are created on the top and bottom surfaces of the beam and are separated by an elastic core. As the pressure is increased the plastic zones grow inwardly until they meet, at which point the thickness of the elastic core is reduced to zero. This configuration is normally termed a plastic hinge. It allows unrestrained plastic deformation that essentially transforms the original clamped boundary condition into a moment-free boundary condition (see Lubliner (1990)). For the clamped plate, the plastic hinge also marks the transition from plate to shell theory as the unrestrained plastic flow allows the redistribution of stresses to a purely tensile hoop stress distribution; in this case, the out-of-plane pressure loading is resisted by membrane stresses. In general, of course, one would have to examine this situation numerically to make definitive statements about the transition of the stress distributions.

After the formation of plastic hinges, the new configuration is that of a curved (elastic) geometry of uniform thickness and under uniform pressure; the boundary conditions are zero displacement and moment and are applied at the circular rim. As the pressure is increased under these circumstances the material adjacent to the concave surface becomes plastic as the initial yield pressure is reached. Held in place by the outer elastic sheath, however, it is unable to flow (see Fig. 2). Flow can only take place when the material becomes fully plastic, which will occur for some higher value of the pressure difference. For an unconstrained cylindrical shell, once a fully plastic state is established there is no stable equilibrium configuration for an infinitesimal increment of pressure since as the shell expands it has a larger radius of curvature, which (as we shall see) reduces its ability to resist the internal pressure. However, for a shell that is constrained (in this case by the rim of the mould), if the shell reshapes into a geometry with a smaller radius of curvature then there is a stable equilibrium configuration even for a shell with reduced thickness (as an isochoric plastic deformation rule would dictate). It is this concept of a sequence of quasi-static changes of equilibrium configuration upon which our model is based.

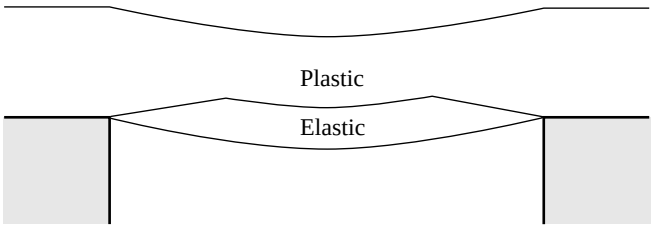

FIG. 2. Schematic diagram showing the elastic and plastic regions of the sheet for pressures between the yield pressure (at which a plastic region first forms) and the flow pressure (at which the sheet is fully plastic)

In Section 2 we motivate the asymptotic approximation of a general shell by considering the simpler problem of an unconstrained circularly cylindrical elastic–plastic shell. This shows how a plastic region forms on the concave side of the shell and gradually expands to cover the entire shell as the pressure is increased. In Section 3 we perform an asymptotic analysis of a general fully plastic shell to identify the equilibrium configurations.

Before proceeding, it is worth assessing the approach adopted in the present work in the light of other existing models. In most of the existing literature it is assumed that superplastic material deforms according to a law of the form

$$\sigma = k\dot{\epsilon}^m, \tag{1}$$

where σ denotes the effective stress, $\dot{\epsilon}$ is the effective strain rate, and k and m are material constants. For superplastic materials $m < 1$ and (1) is conventionally assumed to have been arrived at by means of a suitable 'uniaxial stress test'. The material is therefore treated as a power-law shear-thinning viscous fluid. With this model, the process of superplastic forming becomes equivalent to that of glass blowing, though in the latter the fluid is usually assumed to be Newtonian.

Armed with the material law (1), some authors (see, for example Enikeev & Kruglov (1995)) simplify the problem by making *ad hoc* assumptions about the way that the material might stretch under differential pressure loading, whilst others perform a full finite-element numerical calculation of the solution in three dimensions (Bonet *et al.* (1990), Zhou & Lian (1987), Carrino & Guiliano (1997)). Alternatively, some authors point out that (1) neglects the elastic properties of the material and include the dependence of the stress on the strain as well as the strain rate, some even including the effects of work hardening (Doltsinis (1993), Hu *et al.* (1997)).

Few authors seem to have made systematic use of the fact that the sheet is almost invariably thin by comparison to its lateral dimensions. This is in contrast to the case of glass blowing, for which a simplified model of the evolution of a thin sheet of a Newtonian viscous fluid has been derived systematically in Howell (1996). The power-law case ought to be amenable to a similar treatment.

In the present work we aim to distance ourselves from a description of the material as a power-law fluid, treating it instead as a plastic. Accordingly we suppose that there is a yield stress, below which the material is elastic, and above which it flows plastically. In fact (as we shall see), because we will eventually formulate a quasi-static evolution model where the material progresses through a sequence of steady states, the mechanism of flow

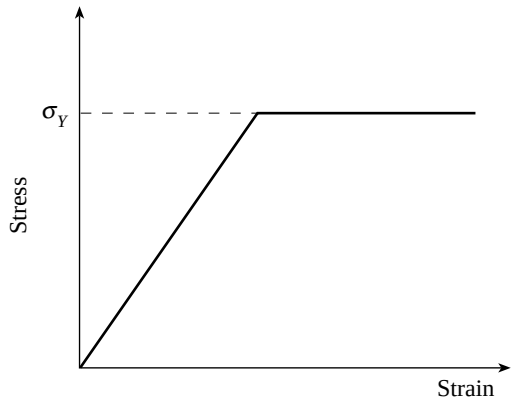

FIG. 3. Stress–strain curve for an elastic/perfectly plastic material

of the material above the yield point is not of paramount importance. We might equally well assume that the material flows as a viscous fluid after yield, as in the case of a Bingham or Herschel–Bulkley fluid. Our approach may therefore be considered as representing the limiting case in which m tends to zero, where a power-law fluid behaves as though it were plastic.

We complete this section by stating the equations governing plastic yield. We will assume that the material is elastic perfectly plastic, so that its stress/strain relationship is as shown in Fig. 3.

Let the stress tensor of the material be denoted by σ_{ij}. This may be written as a sum of the *hydrostatic* stress $\sigma_{kk}\delta_{ij}/3$ (we use the summation convention throughout) and the *deviatoric* stress

$$\sigma'_{ij} = \sigma_{ij} - \sigma_{kk}\delta_{ij}/3.$$

Note that $\sigma'_{kk} = 0$. The Von Mises yield condition for a perfect plastic material may be written (see Hill (1950)) as

$$\sigma'_{ij}\sigma'_{ij} = \frac{2\sigma_Y^2}{3}, \tag{2}$$

where σ_Y is the yield stress of the material in pure (uniaxial) tension.

Coordinate axes may always be chosen so that the stress tensor is diagonal; the coordinate directions are then known as the principal directions and the diagonal entries in the stress tensor as the principal stresses. Let the stress tensor in the principal coordinate system be denoted by τ_{ij}. Then the Von Mises condition (2) may be written in terms of the deviatoric part of the principal stress tensor (see, for example, Calladine (1985) and Hill (1950)) as

$$(\tau'_{11})^2 + (\tau'_{22})^2 + (\tau'_{33})^2 = \frac{2\sigma_Y^2}{3}.$$

This may be rewritten in many ways. Perhaps the most convenient is

$$(\tau_{11} - \tau_{22})^2 + (\tau_{11} - \tau_{33})^2 + (\tau_{22} - \tau_{33})^2 = 2\sigma_Y^2.$$

An alternative plastic yield condition is that due to Tresca (see, for example, Prager (1959)), which is

$$\max\left(|\tau_{11}-\tau_{22}|, |\tau_{11}-\tau_{33}|, |\tau_{22}-\tau_{33}|\right) = \sigma_Y.$$

In two dimensions $\tau'_{33} = 0$, which implies that $\tau_{33} = (\tau_{11}+\tau_{22})/2$. Then the Von Mises condition becomes

$$(\tau_{11}-\tau_{22})^2 = \frac{4\sigma_Y^2}{3},$$

whilst the Tresca condition becomes

$$|\tau_{11}-\tau_{22}| = \sigma_Y.$$

2. Circularly cylindrical shell

In this section we consider the problem of 'inflating' an elastic/plastic cylindrical shell by imposing a slowly increasing internal pressure P. We assume that the displacement of the material is solely radial. The (equilibrium) equations for the stress then become

$$\sigma_{r\theta} = 0, \tag{3}$$

$$r\frac{\partial \sigma_{rr}}{\partial r} + \sigma_{rr} - \sigma_{\theta\theta} = 0, \tag{4}$$

with σ_{rr} and $\sigma_{\theta\theta}$ functions of r only. Whilst the material remains elastic, the stresses are given in terms of the radial displacement u_r by

$$\sigma_{rr} = (\lambda+2\mu)\frac{\partial u_r}{\partial r} + \lambda\frac{u_r}{r}, \tag{5}$$

$$\sigma_{\theta\theta} = \lambda\frac{\partial u_r}{\partial r} + (\lambda+2\mu)\frac{u_r}{r}. \tag{6}$$

These equations must be solved subject to the boundary conditions

$$\sigma_{rr}(a) = -P, \qquad \sigma_{rr}(b) = 0,$$

where a and b are respectively the inner and outer radii of the cylinder. Using the Tresca yield condition, we also have the constraint that $|\sigma_{rr}-\sigma_{\theta\theta}| < \sigma_Y$ for the material to remain elastic (here and for future reference we note that the results for a Von Mises yield condition may be obtained by simply replacing σ_Y with $2\sigma_Y/\sqrt{3}$). Substituting (5), (6) into (4) gives

$$r\frac{\partial^2 u_r}{\partial r^2} + \frac{\partial u_r}{\partial r} - \frac{u_r}{r} = 0 \tag{7}$$

and hence

$$u_r = Ar + \frac{B}{r}. \tag{8}$$

Imposing the boundary conditions now gives

$$\sigma_{rr} = -\frac{a^2P}{b^2-a^2}\left(\frac{b^2}{r^2}-1\right), \tag{9}$$

$$\sigma_{\theta\theta} = \frac{a^2P}{b^2-a^2}\left(\frac{b^2}{r^2}+1\right). \tag{10}$$

The quantity $\Delta = \sigma_{\theta\theta} - \sigma_{rr}$ is given by

$$\Delta = \frac{2a^2b^2P}{r^2(b^2 - a^2)}$$

and is largest on the inner radius, where it is equal to

$$\Delta_a = \frac{2b^2P}{b^2 - a^2}.$$

The cylinder will therefore start to become plastic when the pressure inside reaches the value P_Y given by

$$P_Y = \frac{\sigma_Y(b^2 - a^2)}{2b^2}. \tag{11}$$

For pressures above this value the material comprises a plastic annulus inside an elastic sheath. Let the plastic annulus be $a < r < c$ and the elastic sheath be $c < r < b$. Then equations (3) to (6) and consequently (7) still hold for $c < r < b$, while in $a < r < c$ we have equations (3) and (4) along with the additional condition that

$$\sigma_{\theta\theta} - \sigma_{rr} = \sigma_Y.$$

Hence, for $a < r < c$ we can integrate (4) immediately to give

$$\sigma_{rr} = \sigma_Y \log r + C, \qquad a < r < c.$$

Applying the boundary condition on $r = a$ we obtain

$$\begin{aligned}
\sigma_{rr} &= -P + \sigma_Y(\log r - \log a), \qquad a < r < c,\\
\sigma_{\theta\theta} &= -P + \sigma_Y(\log r - \log a + 1), \qquad a < r < c.
\end{aligned}$$

In the elastic region we still have the solution (8) (with different values of A and B). The normal stress must be continuous across $r = c$ and the material must be at yield, so that the tangential stress at $r = c$ is also zero. The normal stress at $r = b$ is still zero. Applying these conditions gives

$$\begin{aligned}
2(\lambda + \mu)A - \frac{2\mu B}{b^2} &= 0,\\
2(\lambda + \mu)A - \frac{2\mu B}{c^2} &= -P + \sigma_Y(\log c - \log a),\\
2(\lambda + \mu)A + \frac{2\mu B}{c^2} &= -P + \sigma_Y(\log c - \log a + 1),
\end{aligned}$$

for A, B and the position c of the free elastic/plastic boundary. Eliminating A and B gives the following transcendental equation for c:

$$\frac{P}{\sigma_Y} = \log(c/a) + \frac{b^2 - c^2}{2b^2}, \tag{12}$$

the solution of which is shown in Fig. 4 for $a = 1$, $b = 2$. The right-hand side of this

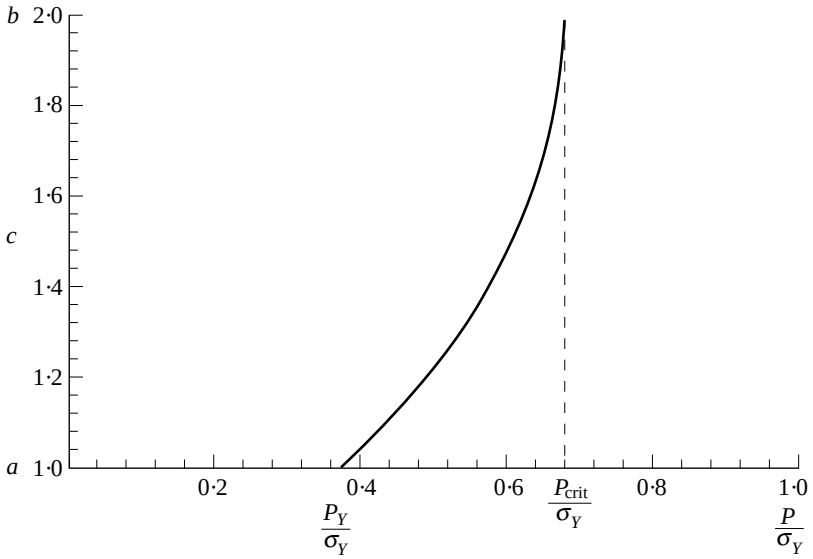

FIG. 4. The boundary of the plastic region, c, as a function of the pressure P ($a = 1$, $b = 2$)

equation increases for c between a and b. Thus, as P increases above P_Y the free boundary moves from $c = a$ to eventually reach $c = b$ when

$$P = P_{\text{crit}} = \sigma_Y \log(b/a). \tag{13}$$

For values of P above P_{crit} the entire cylinder flows plastically and will burst.

To motivate the asymptotics to follow, let us examine the above elastic/plastic solution in the 'thin sheet' limit $b - a \ll 1$. Let $b = a + \epsilon d$ and $r = a + \epsilon\rho$ with $\epsilon \ll 1$. Then, from (9), (10) we see that

$$\sigma_{rr} \sim -P(d - \rho)/d, \tag{14}$$

$$\sigma_{\theta\theta} \sim aP/\epsilon d, \tag{15}$$

while from (11) we see that P_Y is given by

$$P_Y = \sigma_Y \epsilon d/a.$$

The pressure required to generate a plastic zone is thus $O(\epsilon\sigma_Y)$, and the stress in the shell is primarily a hoop stress.

Let us now examine the plastic/elastic solution. From (13) we see that to leading order

$$P_{\text{crit}} \sim \sigma_Y \epsilon d/a.$$

Thus $P_{\text{crit}} = P_Y$ to leading order in ϵ and we must proceed to second order to examine the transition from purely elastic to purely plastic behaviour. Therefore we set $P = \epsilon\sigma_Y d/a + \epsilon^2 \bar{P}$. We also let $c = a + \epsilon\bar{c}$. Then, to leading order throughout the sheet the solution

(14), (15) holds. The quantity of interest is $\bar{c}$, which identifies the point of plastic/elastic transition. Expanding (11) and (13) to two terms gives

$$P_Y \sim \frac{\sigma_Y \epsilon d}{a} - \frac{3\sigma_Y \epsilon^2 d^2}{2a^2},$$
$$P_{\text{crit}} \sim \frac{\sigma_Y \epsilon d}{a} - \frac{\sigma_Y \epsilon^2 d^2}{2a^2}.$$

From (12) we find that $\bar{c}$ is given in terms of $\bar{P}$ by

$$\frac{\bar{P}}{\sigma_Y} \sim -\frac{(\bar{c}-d)^2}{a^2} - \frac{d^2}{2a^2}.$$

3. Arbitrary cylindrical geometry

With the intention of generalizing the work of Section 2, let us now examine a portion of a thin cylindrical sheet of arbitrary thickness and shape. We first note that in the previous sections to leading order the pressure required to initiate a plastic region in the material, P_Y, was the same as that corresponding to a fully plastic material, P_{crit}. Suppose that the pressure on the sheet is increased until it becomes plastic and flows. As it flows it will become more curved, and we have seen that the critical pressure P_{crit} increases with curvature. The sheet will therefore stop flowing when the shape is such that a thin elastic sheath forms on the outside of the sheet. If the pressure is increased further the sheet will again flow, but it will always stop flowing when the pressure is exactly the critical pressure for that shape of sheet. Thus we might expect the sheet to move quasi-statically through critically plastic solutions as the pressure is increased, that is, through solutions in which the whole sheet is plastic and the pressure is exactly equal to the critical pressure P_{crit}.

We are therefore led to ask which shapes are critically plastic for a given pressure.

We begin by making the equations non-dimensional. Henceforth we use a subscript $*$ to represent dimensional variables, whilst unsubscripted variables denote non-dimensional variables. We scale the lengths h_*, R_*, l_* and x_* with the mould semi-width a_*, stresses with the material yield stress σ_Y and pressure with $\epsilon\sigma_Y$, where $\epsilon = \bar{d}_*/a^* \ll 1$ and $\bar{d}_*$ is a typical thickness of the sheet. Thus the dimensionless thickness of the sheet is given by ϵd, where d is an order-one function of position and time.

A curvilinear coordinate system (s, n) is defined by

$$\boldsymbol{x} = \boldsymbol{X}(s) + n\boldsymbol{n},$$

where $\boldsymbol{X}(s)$ is the top (that is, high-pressure) edge of the sheet, s is arc length, and $\boldsymbol{n}$ is the unit normal, which we take to point from the high-pressure region to the low-pressure region. Then

$$\boldsymbol{x}_s = \boldsymbol{X}_s + n\boldsymbol{n}_s = (1+\kappa n)\boldsymbol{t},$$
$$\boldsymbol{x}_n = \boldsymbol{n},$$

where $\boldsymbol{t}$ is the unit tangent and κ is the curvature of the centreline, positive if the centre of curvature lies in the high-pressure region. Our coordinate system is therefore orthogonal,

with scaling factors given by

$$h_1 = 1 + \kappa n, \qquad h_2 = 1$$

where the indices 1 and 2 have been used for the tangent and normal directions respectively.

In these curvilinear coordinates the equations of equilibrium, which represent force balances in the $\boldsymbol{t}$ and $\boldsymbol{n}$ directions, are (see, for example, Chung (1988) or Howell (1994))

$$\frac{\partial}{\partial s}(\sigma_{11}) + \frac{\partial}{\partial n}(h_1\sigma_{12}) + \frac{\partial h_1}{\partial n}\sigma_{12} = 0, \tag{16}$$

$$\frac{\partial}{\partial s}(\sigma_{12}) + \frac{\partial}{\partial n}(h_1\sigma_{22}) - \frac{\partial h_1}{\partial n}\sigma_{11} = 0. \tag{17}$$

We now exploit the fact that the sheet is thin, by rescaling using $n = \epsilon\rho$ where $\epsilon \ll 1$ and asymptotically expanding as $\epsilon \to 0$. We find that (16), (17) become

$$\frac{\partial}{\partial s}(\sigma_{11}) + \frac{1}{\epsilon}\frac{\partial}{\partial \rho}((1 + \kappa\epsilon\rho)\sigma_{12}) + \kappa\sigma_{12} = 0, \tag{18}$$

$$\frac{\partial}{\partial s}(\sigma_{12}) + \frac{1}{\epsilon}\frac{\partial}{\partial \rho}((1 + \kappa\epsilon\rho)\sigma_{22}) - \kappa\sigma_{11} = 0, \tag{19}$$

with boundary conditions

$$\sigma_{22} = 0, \qquad \sigma_{12} = 0 \quad \text{on } \rho = d, \tag{20}$$

$$\sigma_{22} = -\epsilon P, \qquad \sigma_{12} = 0 \quad \text{on } \rho = 0. \tag{21}$$

Expanding in powers of ϵ we set

$$\sigma_{11} = \sigma_{11}^{(0)} + \epsilon\sigma_{11}^{(1)} + \ldots,$$

and use similar expressions for σ_{12} and σ_{22}. Substituting into (18), (19) gives at leading order

$$\frac{\partial \sigma_{12}^{(0)}}{\partial \rho} = 0, \qquad \frac{\partial \sigma_{22}^{(0)}}{\partial \rho} = 0.$$

The boundary conditions then imply that

$$\sigma_{12}^{(0)} = 0, \qquad \sigma_{22}^{(0)} = 0.$$

At next order in (19) we find that

$$\frac{\partial \sigma_{22}^{(1)}}{\partial \rho} = \kappa\sigma_{11}^{(0)}.$$

The Tresca condition for the film to be in the plastic state is

$$|\sigma_{11} - \sigma_{22}| = 1$$

and thus, at leading order,

$$\sigma_{11}^{(0)} = \pm 1.$$

As in the circular case discussed above we find that the predominant stress in the sheet is a hoop stress. Since the sheet is in tension we have

$$\sigma_{11}^{(0)} = 1,$$

and thus (using (20))

$$\sigma_{22}^{(1)} = \kappa(\rho - d).$$

The boundary condition (21) now gives

$$P = d\kappa. \tag{22}$$

Thus, as one might have expected, the sheet behaves exactly as though it were a membrane with tension σ_Y.

Equation (22) is the equation of equilibrium for a curved sheet of arbitrary thickness under a given pressure differential. To formulate a quasi-static evolution model we need equations to describe how the sheet thins and stretches as the pressure is increased.

Let the position of the sheet be given parametrically by

$$\boldsymbol{x} = (x(s,t), y(s,t))$$

where s and t are arbitrary parameters. Conservation of area implies that as this curve lengthens the sheet will thin according to the equation

$$d(s,t)\left(x_s^2 + y_s^2\right)^{1/2} = d_0(s),$$

where d_0 is the initial thickness of the sheet (not necessarily uniform). Finally, we need an equation to say how the curve stretches. We assume that the material flows normal to the curve. This gives the final equation

$$(x_s, y_s) \cdot (x_t, y_t) = 0.$$

Thus, our quasi-static evolution model is

$$\kappa d = P, \tag{23}$$

$$d\left(x_s^2 + y_s^2\right)^{1/2} = d_0, \tag{24}$$

$$x_s x_t + y_s y_t = 0. \tag{25}$$

Using the expression

$$\kappa = \frac{x_s y_{ss} - y_s x_{ss}}{(x_s^2 + y_s^2)^{3/2}},$$

we finally derive, as our model for the quasi-static evolution of a sheet,

$$\frac{d_0(x_s y_{ss} - y_s x_{ss})}{(x_s^2 + y_s^2)^2} = P, \tag{26}$$

$$x_s x_t + y_s y_t = 0; \tag{27}$$

we shall normally specify initial conditions (see further comments below) and end conditions, which for practical purposes will amount to the fact that the ends of the sheet are fixed. In (26) P is a given function of time, but in fact we may take $P = t$ without loss of generality. In some circumstances it is better to think of P as an increasing parameter and to write equation (27) as

$$x_s x_P + y_s y_P = 0.$$

As far as the s-parametrization is concerned, if $d_0(s) = d(s, 0)$ then clearly s is arc length. Often, however, it is more convenient to choose the initial parametrization so that $d_0(s) = 1$ and $(x_s^2 + y_s^2) = d(s, 0)^{-2}$. In this manner (which has been used in much of the work described below) d_0 may be conveniently removed from the problem.

4. Simplified problems

Before we proceed to consider the full problem (26), (27), we attempt to gain some insight into the behaviour of the model by considering two simplified problems. In the first we ignore the thinning of the sheet completely, so that d in (23) is assumed always to be equal to d_0. In the second we apply the condition of conservation of area globally rather than locally, and assume that d is uniform in space.

We consider the problem of an initially flat sheet being sucked into a rectangular mould, as shown in Fig. 5.

4.1 *Constant d*

If d is taken to be constant, then the shapes of the sheet are simply arcs of circles. Due to the non-dimensionalization we may set $d = 1$ without loss of generality. Then, if the instantaneous radius of curvature is R, and the depth of deflection is h, we have (see Fig. 5)

$$h = R - \sqrt{R^2 - 1}, \tag{28}$$

$$R = 1/P, \tag{29}$$

and therefore

$$h = \frac{1}{P} - \sqrt{\frac{1}{P^2} - 1},$$

which is shown graphically (in dimensional form) in Fig. 6. For small P, the initial deflection is given approximately by

$$h \sim \frac{P}{2} + \frac{P^3}{8},$$

which in dimensional variables is

$$h_* \sim \frac{a_*^2}{2}\frac{P_*}{\bar{d}_*\sigma_Y} + \frac{a_*^4}{8}\left(\frac{P_*}{\bar{d}_*\sigma_Y}\right)^3; \tag{30}$$

the deflection of the sheet is thus quadratic in the semi-width a_* to leading order.

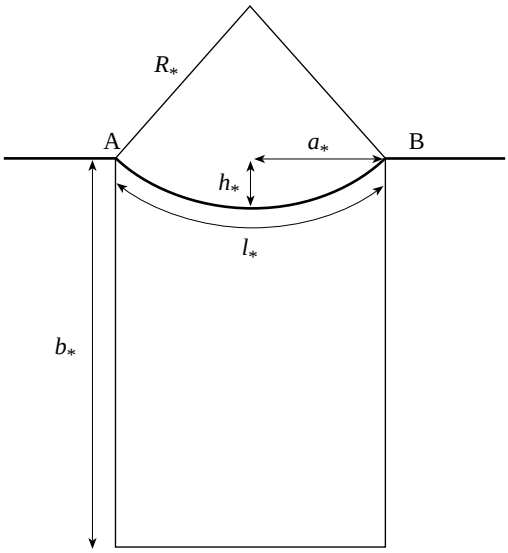

FIG. 5. The geometry of the sheet (dimensional variables)

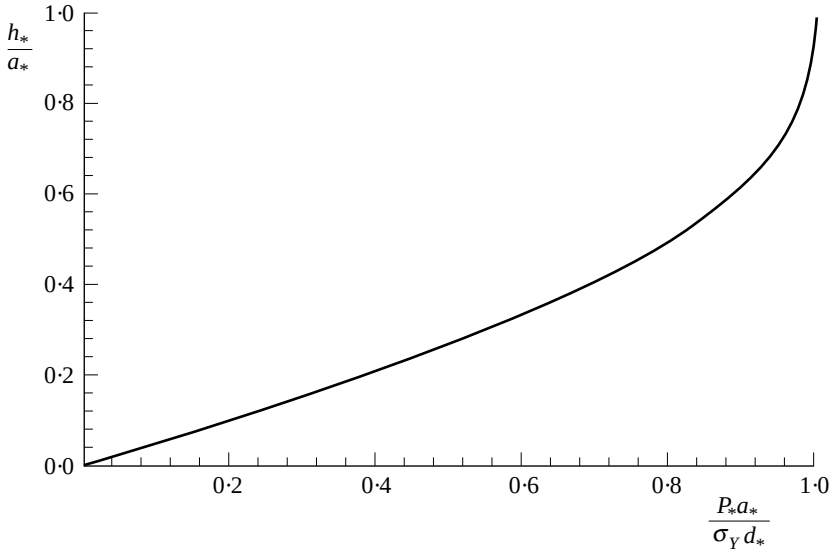

FIG. 6. Dimensionless displacement as a function of dimensionless pressure

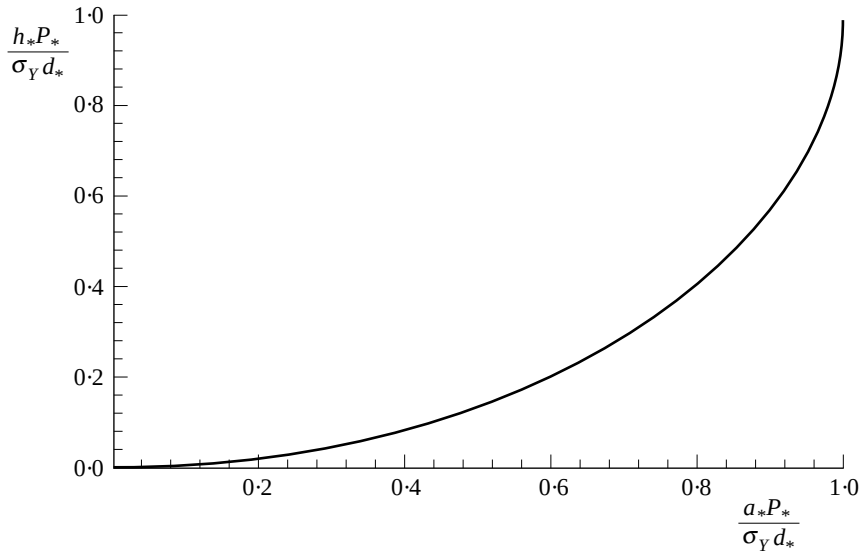

FIG. 7. Dimensionless displacement as a function of dimensionless semi-width

A second quantity of interest is the relationship between the displacement h_* and the semi-width a_* for various pressures. To this end we note that (28), (29) imply that

$$\frac{P_* h_*}{\bar{d}_* \sigma_Y} = 1 - \sqrt{1 - \frac{1}{R^2}}, \tag{31}$$

$$\frac{P_* a_*}{\bar{d}_* \sigma_Y} = \frac{1}{R}. \tag{32}$$

The non-dimensional quantities of interest are therefore

$$\frac{P_* h_*}{\bar{d}_* \sigma_Y} \quad \text{and} \quad \frac{P_* a_*}{\bar{d}_* \sigma_Y}.$$

The relationship (31), (32) is plotted in Fig. 7; it is of interest to note the scaling law implied by (31) and (32), which indicates that the graphs of h_* versus a_* for different pressures can all be collapsed onto a single graph.

4.2 *Uniform d*

We now suppose that the thickness of the sheet is still uniform, but that the sheet thins by mass conservation. Then, for a given deflection, the thickness is determined by the equation

$$ld = 2,$$

where l is the length of the sheet, and again without loss of generality we have taken the initial thickness to be unity. Since d is uniform the shapes of the sheet are still arcs of circles.

Using the same notation as above we have

$$l = 2R\sin^{-1}(1/R),$$
$$d = \frac{1}{R\sin^{-1}(1/R)},$$
$$h = R - \sqrt{R^2 - 1}, \tag{33}$$
$$P = \frac{1}{R^2\sin^{-1}(1/R)}. \tag{34}$$

If we again examine the initial deflection for small P (large R) we find that

$$h \sim \frac{1}{2R} + \frac{1}{8R^3}, \qquad P \sim \frac{1}{R} - \frac{1}{6R^3}.$$

Hence

$$h \sim \frac{P}{2} + \frac{5P^3}{24},$$

or, in dimensional variables,

$$h_* \sim \frac{a_*^2}{2}\frac{P_*}{\bar{d}_*\sigma_Y} + \frac{5a_*^4}{24}\left(\frac{P_*}{\bar{d}_*\sigma_Y}\right)^3. \tag{35}$$

Comparing (35) to (30) we see that the thinning does not alter the first term in the expansion, but does give a greater deflection in the second term, as might be expected.

Displacement is plotted against pressure in Fig. 8. We see that the graph turns around on itself, so that for values of P greater that a critical value P_c there is no solution. This criticality arises because the increase in pressure that the sheet can withstand due to its increase in curvature is less than the decrease in pressure due to the fact that it thins. As P increases through P_c one would expect there to be a large change in the shape of the sheet, which would flow until it touched the base of the mould (this is similar to the instability of the circularly cylindrical shell above the critical pressure P_{crit}).

The value of P_c may be calculated from (33), (34). We find that the critical point corresponds to

$$R_c \approx 1{\cdot}08813, \qquad P_c \approx 0{\cdot}724611, \qquad h_c \approx 0{\cdot}659150,$$

which gives, in dimensional variables,

$$R_{*c} = 1{\cdot}08813\,a_*, \qquad P_{*c} = \frac{0{\cdot}724611\,\sigma_Y\bar{d}_*}{a_*}, \qquad h_{*c} = 0{\cdot}659150\,a_*.$$

It is again of interest to examine the displacement as a function of the semi-width. We find that

$$\frac{h_*P_*}{\bar{d}_*\sigma_Y} = \frac{R - \sqrt{R^2 - 1}}{R^2\sin^{-1}(1/R)}, \tag{36}$$
$$\frac{a_*P_*}{\bar{d}_*\sigma_Y} = \frac{1}{R^2\sin^{-1}(1/R)}. \tag{37}$$

Thus the same scaling law as when d is constant holds, so that the curves for different pressures can be collapsed to a single curve by plotting the correct non-dimensional parameters. The curves (36), (37) are shown in Fig. 9.

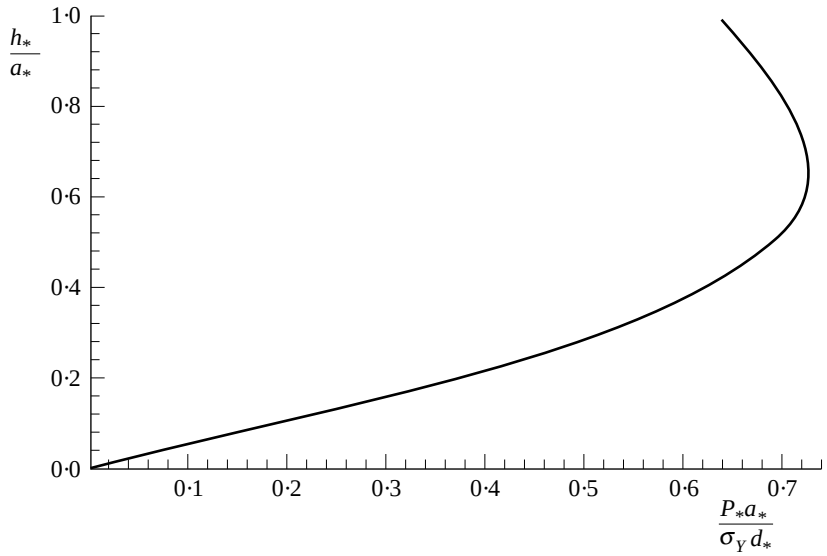

FIG. 8. Dimensionless displacement as a function of dimensionless pressure

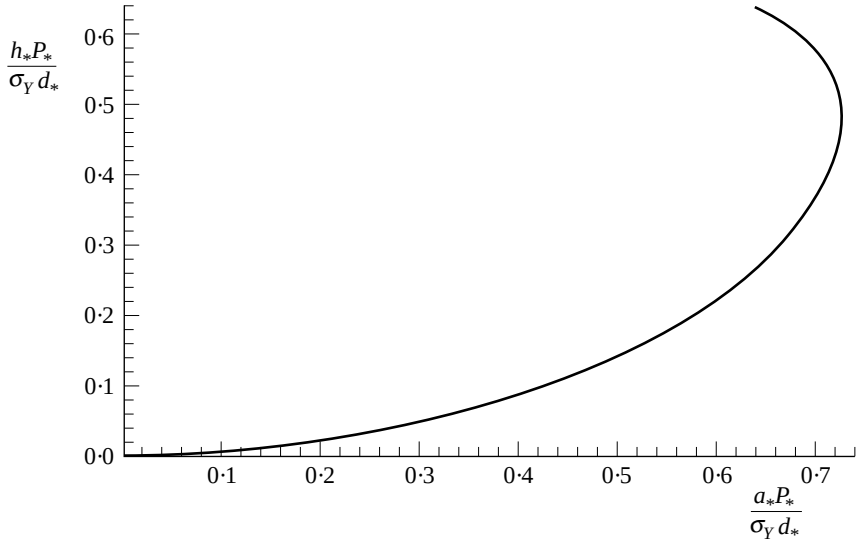

FIG. 9. Dimensionless displacement as a function of dimensionless semi-width

5. Alternative formulation and similarity solutions

It is always useful to obtain some explicit non-trivial solutions of a problem for use as a test for possible numerical schemes. To this end we consider in this section similarity solutions of the problem (23) to (25). We first recast the equations in an alternative form.

Choosing the parametrization for simplicity so that $d_0(s) = 1$ (see remarks at the end of Section 3), we begin by differentiating (24) with respect to s to give

$$d_s = -\frac{x_s x_{ss} + y_s y_{ss}}{(x_s^2 + y_s^2)^{3/2}}. \tag{38}$$

Now we solve the simultaneous equations (38) and (26) for x_{ss} and y_{ss} to give

$$x_{ss} = -\frac{P y_s}{d^2} - \frac{d_s x_s}{d}, \qquad y_{ss} = \frac{P x_s}{d^2} - \frac{d_s y_s}{d}.$$

These may be written as

$$(d x_s)_s = -\frac{P y_s}{d}, \tag{39}$$

$$(d y_s)_s = \frac{P x_s}{d}. \tag{40}$$

Now we differentiate (25) with respect to s, simplify using (23) and solve the resulting equation simultaneously with (25) for x_t and y_t to give

$$x_t = \frac{y_s(x_{st} x_s + y_{st} y_s)}{P(x_s^2 + y_s^2)^2},$$

$$y_t = -\frac{x_s(x_{st} x_s + y_{st} y_s)}{P(x_s^2 + y_s^2)^2}.$$

Differentiating with respect to s again, these may be written as

$$P x_{st} = -(y_s d d_t)_s, \tag{41}$$

$$P y_{st} = (x_s d d_t)_s. \tag{42}$$

Thus our system of equations has become (39), (40); (41), (42); and

$$d(x_s^2 + y_s^2)^{1/2} = 1, \tag{43}$$

not all of which are independent. Now, from (43) we may set

$$d x_s = \cos\phi, \qquad d y_s = \sin\phi,$$

to give

$$d^2 \phi_s = P, \qquad P\phi_t = d d_{st}.$$

As before, we may replace P by t without loss of generality to give

$$\begin{aligned} d^2 \phi_s &= t, \\ t\phi_t &= d d_{st}. \end{aligned} \tag{44}$$

We now examine the similarity solutions of this system. Eliminating d we have

$$\phi_{sst} - \frac{3\phi_{ss}\phi_{st}}{2\phi_s} + 2\phi_s^2\phi_t + \frac{\phi_{ss}}{2t} = 0.$$

This equation has similarity solutions of the form

$$\phi = \phi(\eta), \qquad \eta = st^{\lambda}$$

for any λ, giving

$$\eta\lambda\phi''' + \frac{(\lambda+1)\phi''}{2} - \frac{3\eta\lambda(\phi'')^2}{2\phi'} + 2\eta\lambda(\phi')^3 = 0,$$

where a prime means differentiation with respect to η. Now letting $\phi' = f/\eta$, and $\zeta = \log\eta$ gives

$$\lambda f_{\zeta\zeta} + \frac{(\lambda+1)f_\zeta}{2} - \frac{f}{2} - \frac{3\lambda f_\zeta^2}{2f} + 2\lambda f^3 = 0.$$

Finally, letting $g = f_\zeta/f^{3/2}$ and $\xi = f^{1/2}$ we obtain

$$\xi^3\lambda g g_\xi + (\lambda+1)\xi g - 1 + 4\lambda\xi^4 = 0. \tag{45}$$

This equation does not appear to possess closed-form solutions for general values of λ. The (somewhat degenerate) case with $\lambda = 0$ leads to solutions of the form

$$x = \frac{1}{\sqrt{At}}\sin(As + B) + C,$$

$$y = -\frac{1}{\sqrt{At}}\cos(As + B) + C,$$

where A, B and C are arbitrary constants, but these are unstable and so are of little use for numerical validation. If, however, we now choose $\lambda = -1$ then (45) is separable and integrates to give

$$g^2 = \frac{1}{\xi^2} - 4\xi^2 + a.$$

Substituting for g and ξ in terms of f and integrating gives

$$e^{\zeta} = \frac{bf}{2 + af + 2(1 + af - 4f^2)^{1/2}},$$

which gives

$$\phi' = \frac{4b}{(a\eta - b)^2 + 16\eta^2},$$

so that

$$\phi = -\tan^{-1}\left(\frac{4\eta}{a\eta - b}\right),$$

where the constant of integration has been set to zero, since constants in ϕ correspond simply to a rotation of coordinates. Hence

$$dx_s = \frac{a\eta - b}{((a\eta - b)^2 + 16\eta^2)^{1/2}}, \qquad dy_s = -\frac{4\eta}{((a\eta - b)^2 + 16\eta^2)^{1/2}}.$$

Now, from equation (44) we have

$$d = \frac{t((a\eta - b)^2 + 16\eta^2)^{1/2}}{2b^{1/2}},$$

giving

$$x = \frac{\sqrt{b}}{16 + a^2}\left[-8\tan^{-1}\left(\frac{4bt}{abt - s(16 + a^2)}\right) + a\log\left(\frac{(16 + a^2)s^2 - 2abts + b^2t^2}{t^2}\right)\right], \tag{46}$$

$$y = -\frac{\sqrt{b}}{2}\log t - \frac{2\sqrt{b}}{16 + a^2}\left[a\tan^{-1}\left(\frac{4bt}{abt - s(16 + a^2)}\right) + 2\log\left(\frac{(16 + a^2)s^2 - 2abts + b^2t^2}{t^2}\right)\right]. \tag{47}$$

6. Numerical solution of the two-dimensional quasi-static problem

We now consider the numerical solution for general cases of the two-dimensional quasi-static non-uniform thickness problem. Given a prescribed pressure $P(t)$, the equations

$$\frac{x_s y_{ss} - y_s x_{ss}}{(x_s^2 + y_s^2)^2} = P(t), \tag{48}$$

$$x_s x_t + y_s y_t = 0 \tag{49}$$

must be solved subject to $\boldsymbol{x} = (x_0(s), y_0(s))$ being prescribed at $t = 0$. We assume that, if the parameter s ranges over the values $[s_0, s_1]$ say, then the quantities $(x(s_0, t), y(s_0, t))$ and $(x(s_1, t), y(s_1, t))$ are known. (In cases of industrial relevance, of course, the edges of the sheet will normally be pinned.) There are many possible numerical schemes for solving (48) and (49); the scheme described below has proved to be robust and economical and, with some modifications, could be extended to cover three-dimensional cases.

We seek to discretize (48) and (49) in a semi-implicit manner so that, whilst the method might involve solving systems of linear equations, we are not faced with the complications of dealing with large systems of nonlinear equations. Explicit discretizations are also possible: some numerical experiments have shown, however, that such methods are likely to require a prohibitively small time step for stability.

The particular form of discretization chosen for the equations amounts to using central differences in the evolution equation and evaluating second derivatives in the curvature equation (48) at the new time level. Dividing $[s_0, s_1]$ into N equal intervals each of width $\Delta s = (s_1 - s_0)/N$ and denoting successive time steps of duration Δt by a superscript n, we write $x_k^n = x(s_0 + k\Delta s, n\Delta t)$ $(n \geqslant 0, 0 \leqslant k \leqslant N)$ and discretize (48) and (49) using

$$(x_{k+1}^n - x_{k-1}^n)(y_{k+1}^{n+1} - 2y_k^{n+1} + y_{k-1}^{n+1}) - (y_{k+1}^n - y_{k-1}^n)(x_{k+1}^{n+1} - 2x_k^{n+1} + x_{k-1}^{n+1})$$

$$= \frac{P(t^{n+1})}{8\Delta s}((x_{k+1}^n - x_{k-1}^n)^2 + (y_{k+1}^n - y_{k-1}^n)^2)^2,$$

$$(x_{k+1}^n - x_{k-1}^n)(x_k^{n+1} - x_k^n) + (y_{k+1}^n - y_{k-1}^n)(y_k^{n+1} - y_k^n) = 0.$$

The scheme is applied for $n = 1, 2,\ldots$ and $k = 1, 2,\ldots, N-1$ with x_0^{n+1}, x_N^{n+1}, y_0^{n+1} and y_N^{n+1} known, and yields the linear equations

$$A(\boldsymbol{w}^n)\boldsymbol{w}^{n+1} = \boldsymbol{b}(\boldsymbol{w}^n), \tag{50}$$

where A is the $(2N-2) \times (2N-2)$ matrix with elements given by zero everywhere except for

$$\begin{array}{lll}
A_{i,i} & = X_i & (1 \leqslant i \leqslant N-1), \\
A_{i,i+N-1} & = Y_i & (1 \leqslant i \leqslant N-1), \\
A_{i,i-N+1} & = 2Y_{i-N+1} & (N \leqslant i \leqslant 2N-2), \\
A_{i,i} & = -2X_{i-N+1} & (N \leqslant i \leqslant 2N-2), \\
A_{i,i-N+2} & = -Y_{i-N+1} & (N \leqslant i \leqslant 2N-3), \\
A_{i,i+1} & = X_{i-N+1} & (N \leqslant i \leqslant 2N-3), \\
A_{i,i-N} & = -Y_{i-N+1} & (N+1 \leqslant i \leqslant 2N-2), \\
A_{i,i-1} & = X_{i-N+1} & (N+1 \leqslant i \leqslant 2N-2),
\end{array}$$

where

$$X_k = x_{k+1}^n - x_{k-1}^n, \qquad Y_k = y_{k+1}^n - y_{k-1}^n \qquad (k = 1, 2,\ldots, N-1),$$

the vector $\boldsymbol{b}$ is defined by

$$\begin{array}{lll}
b_i & = x_i^n X_i + y_i^n Y_i & (1 \leqslant i \leqslant N-1), \\
b_N & = R_1 - y_0^{n+1} X_1 + x_0^{n+1} Y_1, & \\
b_i & = R_{i-N+1} & (N+1 \leqslant i \leqslant 2N-3), \\
b_{2N-2} & = R_{N-1} - y_N^{n+1} X_{N-1} + x_N^{n+1} Y_{N-1}, &
\end{array}$$

where

$$R_k = \frac{P(t^{n+1})}{8\Delta s}(X_k^2 + Y_k^2)^2,$$

and

$$w_i = \begin{cases} x_i & (1 \leqslant i \leqslant N-1), \\ y_{i-N+1} & (N \leqslant i \leqslant 2N-2). \end{cases}$$

Assuming that $x = x_0(s)$ and $y = y_0(s)$ are known and $P(t)$, the mould depressurization profile, is given, (50) may be solved using a standard method (in this case we used the NAG routine F04ATF which employs LU factorization with partial pivoting and iterative refinement) to progress from one time step to another. The only other item of practical concern is that the method must somehow be started. At $t = 0$ we require that the profile $\boldsymbol{x} = (x_0(s), y_0(s))$ of the metal plate that is to be extruded must satisfy (48). This is a consequence of the quasi-static nature of the model; if the vacuum forming process

was started with a profile that did not satisfy (48) then $t \to 0$ boundary-layer behaviour (which would perforce be governed by a much more complicated mathematical model) would allow the initial profile to evolve to a state capable of satisfying (48).

When $P(0) = 0$ simple initial plate configurations such as $x_0(s) = s$, $y_0(s) = 0$ are available and may be used: these correspond to metal sheets of constant thickness and so are of practical importance. When $P(0) \neq 0$, however, (48) must be solved numerically to determine $y_0(s)$ for a given $x_0(s)$, say. In the calculations reported below the NAG two-point boundary-value routine D02HAF was used to solve the initial problem. This employs a Runge–Kutta–Merson method and a Newton iteration shooting and matching technique. It is worth noting that the initial problem may also be posed in a number of other ways; if the initial thickness of the metal plate $d_0(s)$ is regarded as given, then the problem to be solved becomes

$$\frac{x_{0s}y_{0ss} - y_{0s}x_{0ss}}{(x_{0s}^2 + y_{0s}^2)^2} = P(t), \tag{51}$$
$$x_{0s}^2 + y_{0s}^2 = d_0^2(s).$$

This could be solved in a similar fashion.

6.1 *Superplastic forming into a mould*

Assume that superplastic forming takes place into a mould bounded by $y = f(x)$. Then clearly when material reaches the mould wall further movement is prevented. Many alternatives are possible to model this behaviour. In the absence of any firm contradictory evidence we make the simplest and most obvious hypothesis, asserting that material sticks to the mould on contact and cannot move thereafter. (It is not obvious that further lateral stretching does not take place; if this were to be observed experimentally then some fairly simple modifications could be built into the model.) The numerical procedure is straightforward: after performing a time step according to (50) each new y_k^{n+1} is examined. If it is found that $y_k^{n+1} < f(x_k^{n+1})$ then linear interpolation is used to ensure that mass is conserved and the calculated values of x_k^{n+1} and y_k^{n+1} are replaced by

$$x_k^{n+1} = \frac{x_k^n f(x_k^{n+1}) - x_k^{n+1} f(x_k^n) + y_k^n x_k^{n+1} - x_k^n y_k^{n+1}}{f(x_k^{n+1}) - f(x_k^n) + y_k^n - y_k^{n+1}},$$
$$y_k^{n+1} = \frac{y_k^n f(x_k^{n+1}) - y_k^{n+1} f(x_k^n)}{f(x_k^{n+1}) - f(x_k^n) + y_k^n - y_k^{n+1}}.$$

6.2 *Numerical stability of the method*

The proposed semi-implicit method was developed in an *ad hoc* fashion: explicit methods were tried and found to be unstable, whilst the nonlinear equations that were produced by fully implicit methods proved costly to solve. As usual in such cases, it is desirable to consider the numerical stability and convergence of the scheme. The nonlinearity of (48) and (49) renders exact analysis prohibitively difficult, however, and the best that may

be accomplished is to investigate the stability properties of a related paradigm system. Examining the system

$$x_t + \lambda y_t = 0, \tag{52}$$

$$y_{ss} - \mu x_{ss} = P(t)(x_s + y_s), \tag{53}$$

where λ and μ are constant and $P(t)$ is given, subject to the discretization

$$x_k^{n+1} - x_k^n + \lambda(y_k^{n+1} - y_k^n) = 0, \tag{54}$$

$$y_{k+1}^{n+1} - 2y_k^{n+1} + y_{k-1}^{n+1} - \mu(x_{k+1}^{n+1} - 2x_k^{n+1} + x_{k-1}^{n+1}) = \tfrac{1}{2}P(t^n)\Delta s(x_{k+1}^n - x_{k-1}^n + y_{k+1}^n - y_{k-1}^n) \tag{55}$$

we find that, written in block matrix form with $\boldsymbol{z}^n = (\boldsymbol{x}^n \mid \boldsymbol{y}^n)^T$, the scheme (54) and (55) amounts to

$$B\boldsymbol{z}^{n+1} = Q\boldsymbol{z}^n + \boldsymbol{G}^n(t).$$

Here $\boldsymbol{G}^n(t)$ is a $2N-2$-vector whose composition is immaterial as far as the numerical stability of the scheme is concerned,

$$B = \begin{pmatrix} I & \lambda I \\ \mu A & -A \end{pmatrix}, \quad Q = \begin{pmatrix} I & \lambda I \\ K & K \end{pmatrix}$$

and

$$A = \begin{pmatrix} 2 & -1 & 0 & \dots & \dots & 0 \\ -1 & 2 & -1 & \dots & \dots & 0 \\ 0 & -1 & 2 & \dots & \dots & 0 \\ \vdots & \vdots & \vdots & \ddots & & 0 \\ \vdots & \vdots & \vdots & -1 & 2 & -1 \\ 0 & 0 & 0 & 0 & -1 & 2 \end{pmatrix}, \quad K = \begin{pmatrix} 0 & k & 0 & \dots & \dots & 0 \\ -k & 0 & k & \dots & \dots & 0 \\ 0 & -k & 0 & \dots & \dots & 0 \\ \vdots & \vdots & \vdots & \ddots & & 0 \\ \vdots & \vdots & \vdots & -k & 0 & k \\ 0 & 0 & 0 & 0 & -k & 0 \end{pmatrix}.$$

The stability of the system is thus determined by the spectral radius $\rho(C)$ of the iteration matrix

$$C = B^{-1}Q = \frac{1}{1+\lambda\mu}\begin{pmatrix} I + \lambda A^{-1}K & \lambda I + \lambda A^{-1}K \\ \mu I - A^{-1}K & \lambda\mu I - A^{-1}K \end{pmatrix}.$$

Denoting the eigenvalues of C by p, it is possible to show by elementary row and column operations that the condition $\det(C - pI) = 0$ is equivalent to

$$\det\begin{pmatrix} (1-p)I & 0 \\ 0 & A^{-1}K - qI \end{pmatrix},$$

where $p = -q/(1+\lambda\mu)$. Since clearly C has $N-1$ eigenvalues given by $p = 1$, its spectral radius is ultimately determined by $\rho(A^{-1}K)$. The spectral radii of A^{-1} and K are easily determined, for the eigenvalues of A^{-1} and K are given respectively by $(2 - 2\cos(j\pi/N))^{-1}$ and $2ik\cos(j\pi/N)$ for $(j = 1, 2, \dots, N-1)$. There seems to be no simple expression, however, for the eigenvalues of $A^{-1}K$. Although the spectral radius of a product is bounded by the product of the spectral radii when both matrices are Hermitian,

this need not be true otherwise. Since K is not Hermitian, we are forced to rely on the bound

$$\rho(M) \leqslant \|M\|$$

which is true for all real matrices M. Luckily, in the present case it transpires that the infinity norm of $A^{-1}K$ is easy to determine; straightforward (though tedious) methods show that

$$\|A^{-1}K\|_\infty = k(N-2).$$

The spectral radius of C is thus 1 (and the method is therefore neutrally stable) provided

$$|\ p\ | \leqslant \frac{(N-2)\Delta s P(t^n)}{2\ |\ 1+\lambda\mu\ |} \leqslant 1.$$

Since $\Delta s = (s_1 - s_0)/N$, this amounts to the condition that

$$\frac{(s_1 - s_0)(1-2/N)P(t^n)}{2\ |\ 1+\lambda\mu\ |} \leqslant 1. \tag{56}$$

Although the requirement (56) ensures the (neutral) stability of the method only for the paradigm linear problem (52) and (53), its conclusions are well borne out in practice for the full problem. Experience using the scheme (50) shows that stability never depends on the size or number of space or time steps, but rather on the size of the pressure $P(t)$. The validation results given below for a test problem are typical and confirm that it is accuracy, rather than stability, that depends upon the mesh details. We also note that, as expected, for a given $x_0(s)$, the initial boundary-value problem (51) may not possess a solution for all $P(0)$; for example, when $x_0(s) = s$ it is straightforward to show that the relevant boundary-value problem has a solution only if

$$P(0) \leqslant \tfrac{1}{2}\pi.$$

6.3 *Method validation*

As indicated above, the stability and accuracy of the method may be analysed only for a linearized version of the problem. Validation of the scheme and numerical code using a test case is therefore important. Using the similarity solution (46), (47) numerical solutions were computed for various values of the parameters a and b and for various spatial and temporal discretizations. In all cases the numerical scheme performed efficiently and accurately. Table 1 shows a typical set of results, computed with $b = 1$ and $a = 0$. Computations were performed starting from $t = 1$ up to a time $t = 11$. For each discretization the quantity $\|\boldsymbol{x}_c - \boldsymbol{x}_e\|_\infty$ is shown, where $\boldsymbol{x}_c$ is the computed solution and $\boldsymbol{x}_e$ the exact solution given by (46) and (47). As predicted by the stability analysis, no spatial or temporal discretization exhibits instability. For a fixed spatial mesh, the error decreases to a minimum as the time step decreases, before increasing again.

A typical set of results for the test problem is illustrated in Fig. 10, where the parameters $N = 50$, $\Delta t = 0{\cdot}005$ were used. The computed solution (solid line) is almost indistinguishable from the exact solution (dotted lines). The only slight noticeable errors are in the thickness near to the ends of the sheet; this is due to the explicit nature of the scheme.

TABLE 1
Error norm for test case using (46) and (47) with $a = 0$, $b = 1$

N	Δt = 0·2	0·1	0·05	0·02	0·01	0·005	0·002	0·001
5	5·2471E-3	1·8129E-3	1·1081E-3	2·1948E-3	2·5641E-3	2·7501E-3	2·8621E-3	2·8996E-3
10	6·7818E-3	3·0212E-3	1·2884E-3	2·9490E-3	4·4155E-4	6·1961E-4	7·2737E-4	7·6345E-4
20	7·8573E-3	3·4660E-3	1·6006E-3	5·6771E-4	2·3708E-4	7·4294E-5	1·3701E-4	1·7185E-4
30	9·2444E-3	3·6997E-3	1·6906E-3	6·2317E-4	2·8749E-4	1·2329E-4	2·5912E-5	5·8335E-5
40	1·4835E-2	3·9385E-3	1·7496E-3	6·4651E-4	3·0610E-4	1·4067E-4	4·2903E-5	1·8232E-5
50	6·9072E-2	4·2424E-3	1·8018E-3	6·6062E-4	3·1552E-4	1·4891E-4	5·0725E-5	1·8397E-5

Finally, we note that because of the method chosen, the equations have a banded structure and are sparse. One consequence of this is that the method would be easily applicable to three dimensions. Using parameters u and v so that the equation of the metal sheet is given by $\boldsymbol{x} = (x(u, v), y(u, v), z(u, v))$, the equations of motion under similar modelling assumptions to those used for the two-dimensional case become

$$x_u x_t + y_u y_t + z_u z_t = 0,$$

$$x_v x_t + y_v y_t + z_v z_t = 0,$$

$$K(u, v)d(u, v)\sigma_Y = P(t),$$

$$d(u, v)(C_{11}C_{22} - C_{12}^2)^{\frac{1}{2}} = d_0$$

where the mean curvature k is given by

$$K = \frac{1}{2(C_{11}C_{22} - C_{12}^2)^{3/2}}[C_{22}(C_6 x_{uu} + C_5 y_{uu} + C_4 z_{uu}) - 2C_{12}(C_6 x_{uv} + C_5 y_{uv} + C_4 z_{uv}) + C_{11}(C_6 x_{vv} + C_5 y_{vv} + C_4 z_{vv})],$$

and

$$C_{11} = x_u^2 + y_u^2 + z_u^2, \qquad C_{12} = x_u x_v + y_u y_v + z_u z_v, \qquad C_{22} = x_v^2 + y_v^2 + z_v^2,$$

$$C_4 = x_u y_v - y_u x_v, \qquad C_5 = z_u x_v - x_u z_v, \qquad C_6 = y_u z_v - z_u y_v.$$

Although if each coordinate direction is discretized using N points (as for the two-dimensional case) we now need to solve a $3(N-1)^2 \times 3(N-1)^2$ system of linear equations; the sparsity of the equations renders them amenable to the use of specific routines to minimize storage and solution time.

Although details of a fully three-dimensional numerical solution must await another study, it is worth pointing out that such a model would allow detailed comparisons with experiment to be made. An extensive search of the literature has failed to find any two-dimensional 'channel' type experiments, thus limiting the current study to qualitative comparisons.

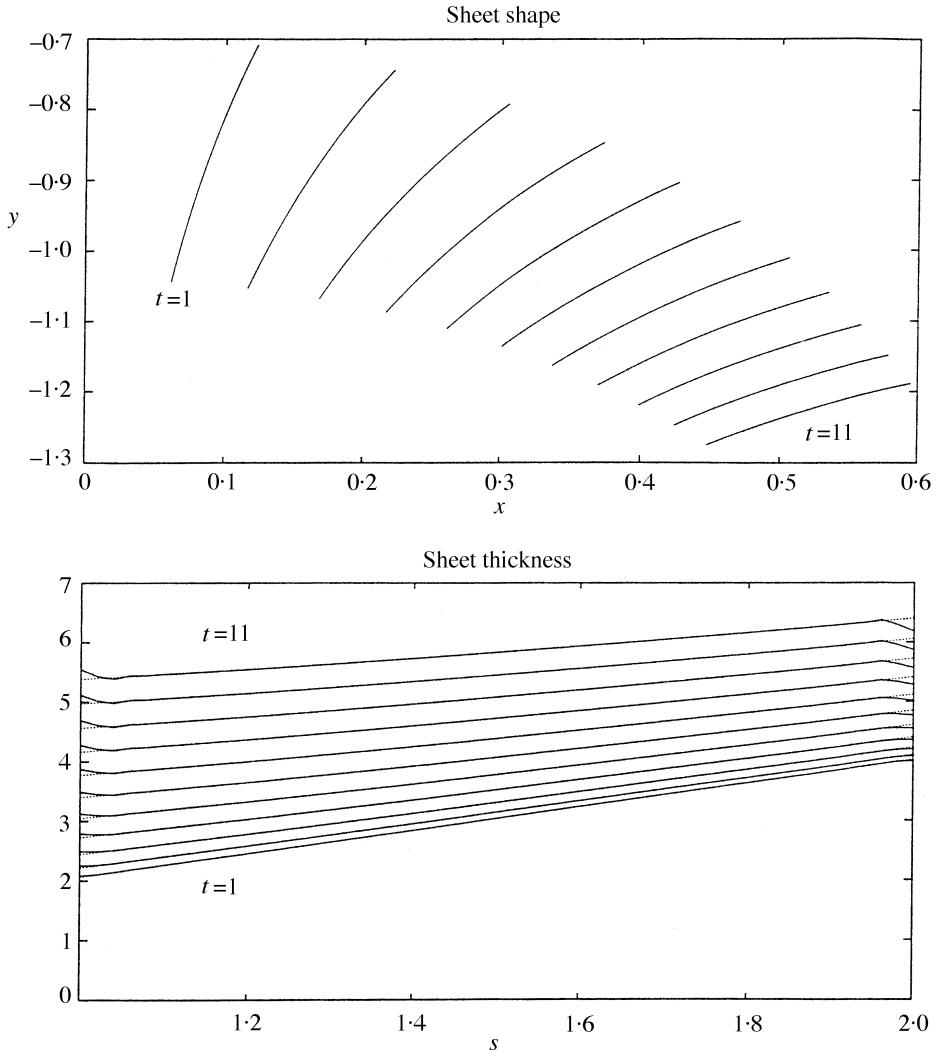

FIG. 10. Numerical (solid lines) vs. exact (dashed lines) solution comparison for test case

7. Numerical results

Numerical solutions to (48) and (49) were computed for a variety of cases. In each of the computations reported below 50 mesh points and a time step $\Delta t = 0{\cdot}001$ were used. Computations took place over the region $1 \leqslant s \leqslant 2$ and for $t > 0$.

Figure 11 shows a typical case of flow with no restraining mould wall; for this case the pressure was given for $t > 0$ by

$$P(t) = 1 - \mathrm{e}^{-t},$$

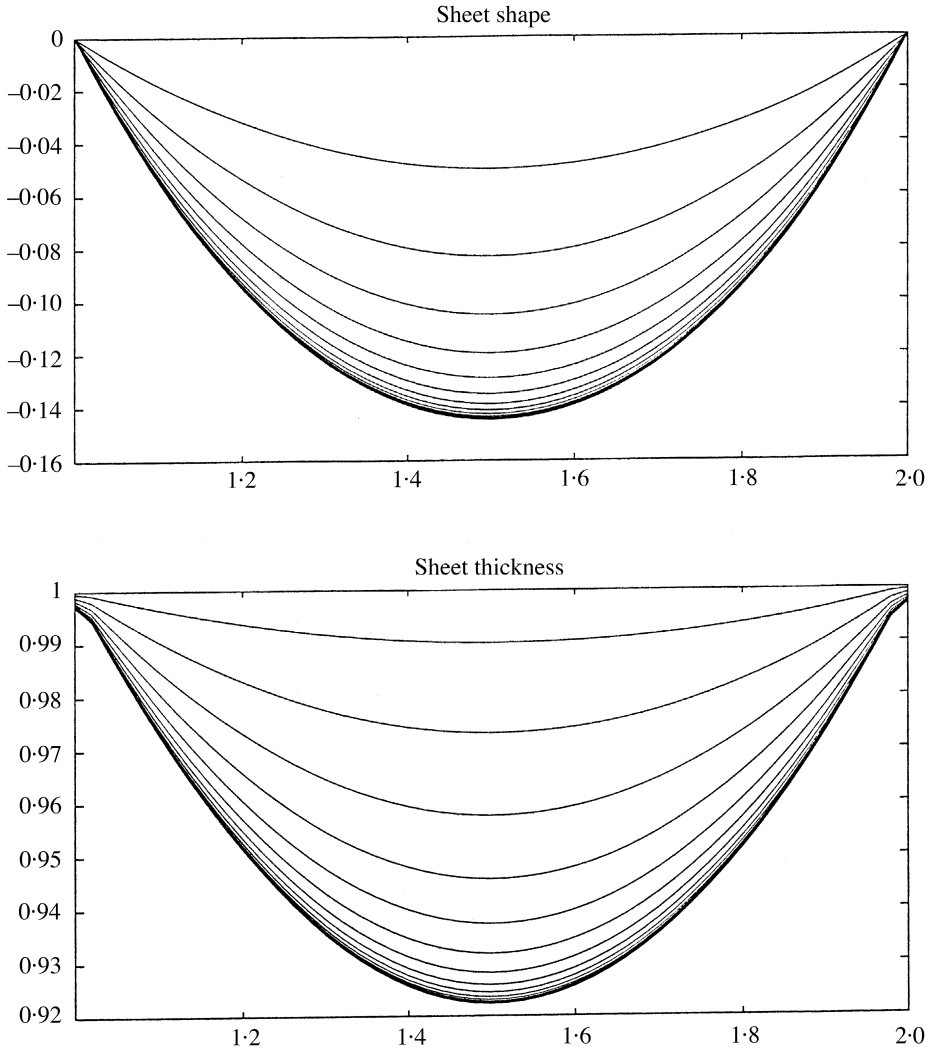

FIG. 11. Superplastic vacuum moulding for $t > 0$ with $P(t) = 1 - e^{-t}$ and an initially constant thickness sheet

the sheet was fixed at the corners (1, 0) and (2, 0), and the initial sheet thickness was given by $x_0(s) = s$, $y_0(s) = 0$ so that $d_0(s) = 1$ everywhere.

The behaviour of the sheet in this case is as one might expect; after an initial rather rapid sheet expansion phase, the ever slower increase in pressure expands the sheet to a final steady-state configuration. Results are shown at intervals of 0·5 time units, and we note that the sheet reaches just over one-half of its maximum downward deflection in a time of 1 and occupies virtually its steady-state position by the time $t = 4$. The sheet thickness is equally predictable, with a maximum thinning of just under 8 per cent at the centre of the sheet.

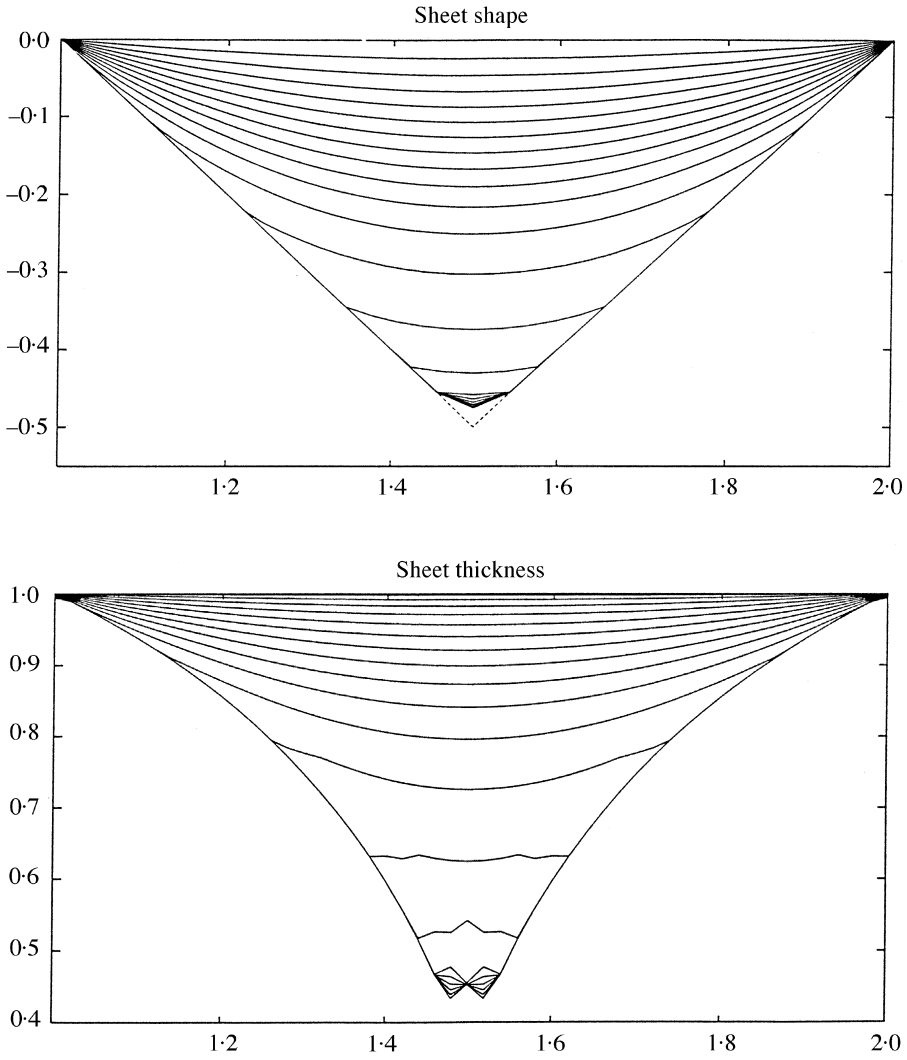

FIG. 12. Superplastic vacuum moulding for $t > 0$ with $P(t) = 2(1 - e^{-t})$ and an initially constant thickness sheet into a wedge-shaped mould

Figure 12 shows superplastic moulding into a mould (shown by a broken curve) defined by

$$y = \begin{cases} -(x-1) & (x < \frac{3}{2}), \\ -(2-x) & (x \geqslant \frac{3}{2}), \end{cases}$$

with a driving pressure

$$P(t) = 2(1 - e^{-t}).$$

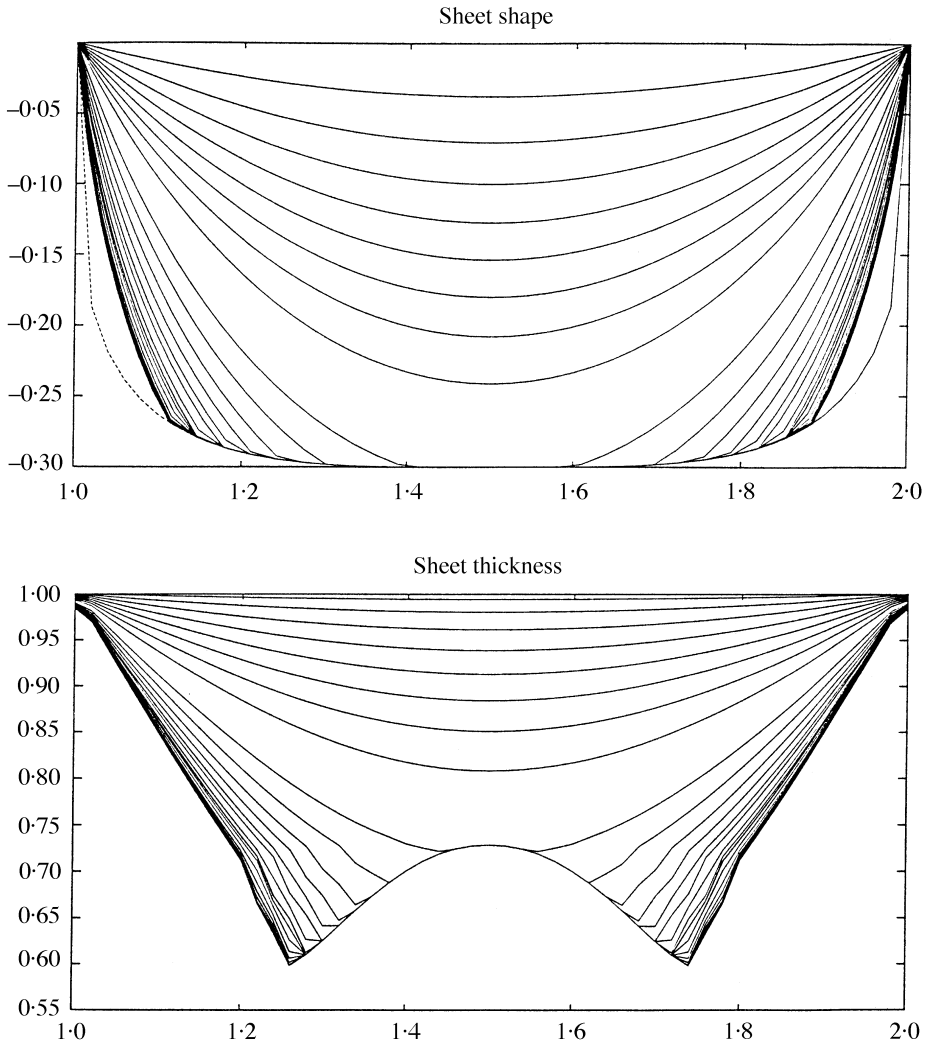

FIG. 13. Superplastic vacuum moulding for $t > 0$ with $P(t) = 1{\cdot}65(1 - e^{-t})$ and an initially constant thickness sheet into a shaped mould

Once again, the sheet was fixed at the corners (1, 0) and (2, 0) and the initial sheet thickness was given by $x_0(s) = s$, $y_0(s) = 0$ so that $d_0(s) = 1$ everywhere. Results are shown at intervals of 0·1 time units. The sheet bends at its corners until it makes contact with the mould wall. Parts of the sheet that are in contact with the wall stick to the mould, whilst the remaining free parts of the sheet are further stretched. Although penetration into the bottom corner of the mould is not complete, the material fails only by a small amount to fill the mould completely. The thinning of the sheet is apparent from the lower section of Fig. 12, as is the characteristic 'W' shape of the thickness of the final product.

One of the anticipated uses of superplasticly moulded zinalco is to form soda cans and other articles used for containing food. In Fig. 13 a driving pressure given by

$$P(t) = 1{\cdot}65(1 - \mathrm{e}^{-t})$$

is used to form a sheet of initially constant thickness into a mould with a container-type shape given by

$$f(x) = -0{\cdot}3(1 - (2x - 3)^4)^{1/4}.$$

Output is shown every 0·2 time units, and though rapid expansion takes place up to and until the centre of the metal sheet reaches the bottom of the mould, expansion is slowed thereafter. Ultimately, the sheet fails to penetrate into the furthest corners of the mould. We also note that the sheet thickness once again assumes a 'W' profile as thinning is partially prevented near to the centre of the sheet by its contact with the mould wall. In contrast to the previous case, however, the 'W' shape of the thickness curve is now much more pronounced. This agrees well with qualitative experimental evidence which suggests that a more pronounced 'W' should be observed whenever the material hits the bottom of the mould before reaching its sides.

8. Conclusions

Based on the hypothesis that a superplastic sheet is in a critically plastic state whenever it stops flowing we have systematically derived a model for the final shape of a sheet subjected to a given pressure-drop history. This model may be thought of as representing the limit $m \to 0$ of the more usual power-law fluid approach to superplastic materials and is derived by performing an asymptotic expansion in the limit as the thickness of the sheet tends to zero.

Some aspects of the model are worth further comment. The model that we obtain is quasi-static, moving through a series of steady states. Such steady states exist because we have assumed that the material possesses a yield stress—in the case of a power-law fluid there would be no steady state until the sheet covered the mould. Much previous published work on superplastic forming has focused on the problem of how to adjust the pressure history so that the strain rate is such that exponent m (which is typically a function of strain rate, so that technically it is incorrect to refer to such materials as power-law fluids) is maximized (Bonet *et al.* (1990), Carrino & Guiliano (1997)). The aim behind this is to minimize the possibility of necking. Since we are concerned here with a quasi-static model, all monotonic pressure histories arriving at the same final pressure drop will have the same final state. However, the numerical stability of the problem indicates that under the assumption of a critically plastic state necking will not occur.

For some superplastic materials m may be as large as 0·8, in which case the limit $m \to 0$ may not be appropriate. The main point at issue for such values of m is the validity of the quasi-static assumption. Even for such materials, however, if the forming process is carried out using rapid pressure drops the theory developed above may still give useful results.

In Section 4 we examined the predictions of this model for the dependence of the final displacement of the sheet on both applied pressure and the dimensions of the opening of the mould, under the assumption that the thickness of the sheet remained uniform. The

analysis highlighted certain non-dimensional groups as being the important parameters; it will be interesting to see if the experimental data can be collapsed onto a single curve by rescaling as this analysis suggests.

Finally, work is presently being carried out to extend the model and numerical scheme to fully three-dimensional cases. This will allow a more direct quantitative comparison with experimental results.

Acknowledgements

The first author was supported by a Royal Society Research Fellowship. The problem arose originally at a joint Industry/University meeting held in Cocoyoc, Mexico in February 1997 organised by ECMI (European Consortium for Mathematics in Industry) and SMM (Sociedad Matemática Mexicana) which was partially funded by the ALFA programme.

REFERENCES

BONET, J., WOOD, R. D., & WARGADIPURA, A. H. S. 1990 Numerical simulation of the superplastic forming of thin sheet components using the finite element method. *Int. J. Num. Meth. Eng.* **30**, 1719–1737.

CALLADINE, C. R. 1985 *Plasticity for Engineers.* Series in Engineering Science. Chichester: Ellis Horwood.

CARRINO, L. & GUILIANO, G. 1997 Modelling of superplastic blow forming. *Int. J. Mech. Sci.* **39**, 193–199.

CHUNG, T. J. 1988 *Continuum Mechanics.* Englewood Cliffs: Prentice-Hall.

DOLTSINIS, I. S. 1993 Numerical analysis and design of industrial superplastic forming. *J. de Physique* IV **3**, 1187–1197.

ENIKEEV, F. U. & KRUGLOV, A. A. 1995 An analysis of the superplastic forming of a thin circular diaphragm. *Int. J. Mech. Sci.* **37**, 473–483.

GREEN, A. E. & ZERNA, W. 1954 *Theoretical Elasticity*. Oxford: Clarendon Press.

HILL, R. 1950 *The Mathematical Theory of Plasticity*. Oxford: University Press.

HOWELL, P. D. 1994 *Extensional thin layer flows*. D. Phil. Thesis, Oxford University.

HOWELL, P. D. 1996 Models for thin viscous sheets. *Euro. J. Appl. Math.* **4**, 321–343.

HU, P., LIU, Y. Q., LI, X., & LIAN, J. 1997 Rigid viscoplastic finite element analysis of the gas-pressure constrained bulging of superplastic circular sheets into cone disk shape dies. *Int. J. Mech. Sci.* **39**, 487–496.

LUBLINER. J. 1990 *Plasticity Theory*. New York: Macmillan.

PRAGER, W. 1959 *An Introduction to Plasticity*. Reading, Massachusetts: Addison–Wesley.

SHERBY, O. D., NIEH, T. G., & WADSWORTH, J. 1994 Overview on superplasticity research on small-grained materials. In: Proceedings of the 1994 International Conference on Superplasticity in Advanced Materials (ICSAM-94), May 24–26, Moscow.

ZHOU, D.-J. & LIAN, J. 1987 Numerical analysis of superplastic bulging for cavity-sensitive materials. *Int. J. Mech. Sci.* **29**, 565–576.